SUPERCONDUCTING GANTRY AND OTHER DEVELOPMENTS AT HIMAC

Y. Iwata[*], K. Noda, T. Shirai, T. Murakami, T. Fujita, T. Furukawa, K. Mizushima, Y. Hara,
S. Suzuki, S. Sato, and K. Shouda, NIRS, 4-9-1 Anagawa, Inage, Chiba 263-8555, Japan
T. Fujimoto, and H. Arai, AEC, 3-8-5 Konakadai, Inage, Chiba 263-0043, Japan
T. Ogitsu, KEK, 1-1 Oho, Tsukuba, Ibaraki 305-0801, Japan
T. Obana, NIFS, 322-6 Oroshi-cho, Toki-city 509-5292, Japan
N. Amemiya, Kyoto Univ., Kyoto-Daigaku-Katsura, Nishikyo, Kyoto 615-8510, Japan
T. Orikasa, S. Takayama, Y. Nagamoto, and T. Yazawa, Toshiba Corp., 1-1-1 Shibaura, Minatoku,
Tokyo 105-8001, Japan

Abstract

New developments at HIMAC include a super-conducting carbon gantry, a new therapy area with three new treatment rooms, and substantial enhancements to the synchrotron extraction system to enable energy-variation through multiple flattops within a synchrotron cycle to match characteristics of the gantry and three-dimensional raster scanning. The carbon gantry consists of ten combined-function superconducting magnets, allowing a very compact geometry – the length and the radius of the gantry are approximately 13 and 5.5 m, respectively, comparable to the dimensions of existing proton gantries. Further, these superconducting magnets are designed for fast slewing of the magnetic field to follow the multiple flattop operation of the synchrotron. In this paper, the recent developments of HIMAC are presented.

INTRODUCTION

Heavy-ion cancer-therapy using the Heavy-Ion Medical Accelerator in Chiba (HIMAC) has been carried out since June 1994. The successful cancer treatments have led us to construct a new treatment facility [1]. The new treatment facility equips with three treatment rooms; two of them have both horizontal and vertical fixed-irradiation-ports, and the other is a rotating gantry port as schematically shown in Fig. 1. For all the ports, the three-dimensional raster-scanning irradiation method with pencil beam will be employed [2].

In raster-scanning irradiation, a target is directly irradiated with high-energy carbon-ions, after being accelerated by a synchrotron ring. Since the position of the focused beam on a target is controlled by the fast horizontal and vertical scanning-magnets, the lateral dose distribution is determined by these scanning magnets. On the other hand, the depth dose-distribution is determined by beam energy. To control the depth dose-distribution, it is preferable to change the beam energy directly by the accelerators, instead of using energy degraders, since energy degraders may broaden the spot size of the beam on a target, and concurrently produce secondary fragments, which could adversely affect the depth dose-distribution.

To quickly change the energy of the beam, as provided by the synchrotron ring, we developed a multiple-energy operation with extended flattops [3]. The proposed operation enables us to provide carbon ions having various energies in a single synchrotron cycle; namely, the beam energy would be successively changed within a single synchrotron pulse. With this operation, the beam range could be controlled without using any energy degraders.

To further obtain precise dose distributions, we developed an isocentric superconducting rotating-gantry for carbon therapy [4]. This rotating gantry is designed to transport carbon ions having 430 MeV/u to an isocenter with irradiation angles of over ±180 degrees, and is further capable of performing the fast raster-scanning irradiation. The combined-function superconducting magnets will be employed for the rotating gantry. Use of the superconducting magnets with optimized beam optics allow a compact gantry design with a large scan size at the isocenter; the length and the radius of the gantry will be approximately 13 and 5.5 m, respectively, which are comparable to those for the existing proton gantries. This rotating gantry is currently under construction, and will be installed in the room G of the new treatment facility.

We report the recent developments of the multiple flattop operation as well as the superconducting rotating-gantry.
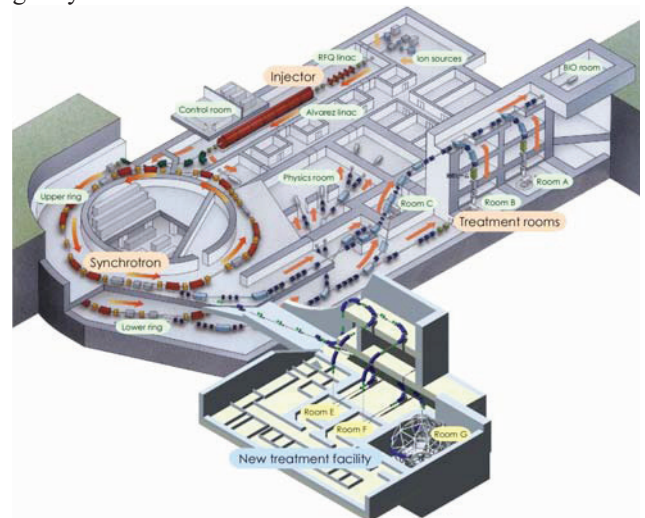

Figure 1: Layout of the HIMAC complex.
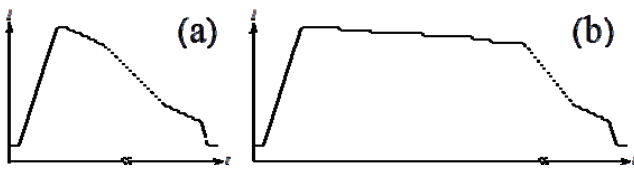
*corresponding author. E-mail: y_iwata@nirs.go.jp (Y. Iwata)

Figure 2: (a) Schematic drawing of synchrotron pattern for multiple-energy operation. (b) The same pattern as (a), but with the extended flattops. The beam is extracted from the synchrotron ring during these extended flattops.
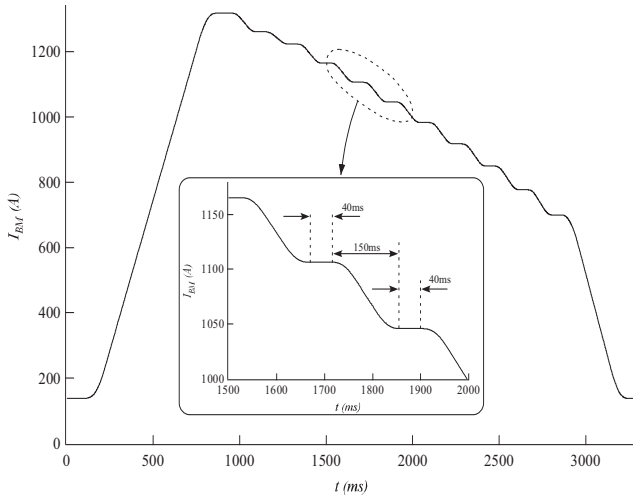

Figure 3: A current pattern for the main-bending magnets in the ring as a function of time. The currents of the 11 flattops correspond to the beam energies of 430, 400, 380, 350, 320, 290, 260, 230, 200, 170, and 140 MeV/u.

MULTIPLE FLATTOP OPERATION

The multiple-energy operation employs operation patterns having a stepwise flattop, as schematically shown in Fig. 2(a). With these operation patterns, the carbon ions injected in the ring are initially accelerated to the maximum energy, and then successively decelerated to lower energies. Although the stepwise pattern only has short flattops, where the beam can be extracted from the ring, we can extend the flattop and extract the beam during the extended flattop.
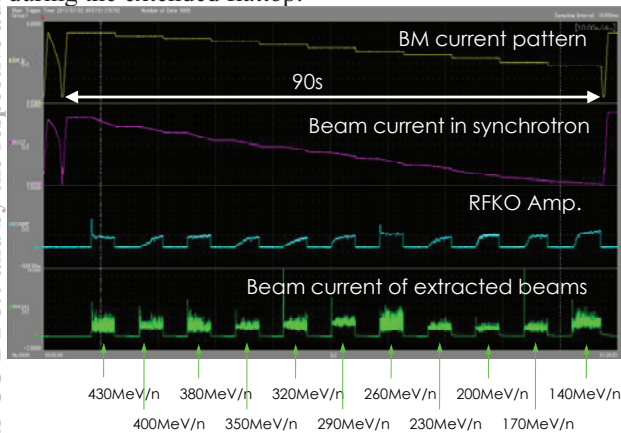

Figure 4: Current patterns for the main bending magnets, beam current in the synchrotron ring, RFKO amplitude, and the beam current of the extracted beam.
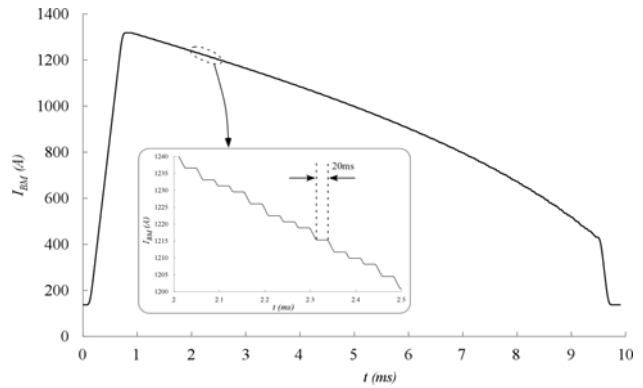
Figure 5: A current pattern for the main-bending magnets in the ring. This pattern has 201 flattops.

Having consecutively extended the flattops, as illustrated in Fig. 2(b), the beams having various energies can be extracted from the ring within a single synchrotron cycle, and hence the total irradiation time can be considerably reduced.

11-flattop pattern

To prove the principle of multiple-energy operation with extended flattops, we have performed beam acceleration and extraction tests using the stepwise operation pattern. In the tests, a current pattern for the main bending magnet having 11 short flattops, corresponding to 11 beam energies, was prepared as shown in Fig. 3. Further, similar patterns were prepared for other devices, such as the main quadrupole, sextupole magnets, the RF-acceleration cavity, and the beam-extraction devices in the extraction channel. By using the prepared operation patterns, the beam will be initially accelerated to 430 MeV/u, and then consecutively decelerated down to 140 MeV/u at an energy step of 20 MeV/u or 30 MeV/u. Results of the beam test are shown in Fig. 4. As can be seen in the figure, beams having 11 different energies were successively extracted from the synchrotron ring. The multiple-energy operation using this pattern was successfully commissioned, and has been used for scanning treatments since FY 2012.

Full energy-scan with 201-flattop pattern

The final goal of this project is to control the depth dose-distribution by varying the beam energy from the accelerators, namely, *full energy scanning*. To accomplish
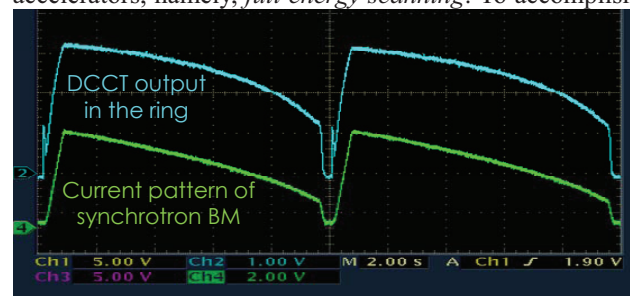

Figure 6: Current patterns for the main bending magnets, DCCT output in the synchrotron ring during beam acceleration tests using the 201-flattop pattern.
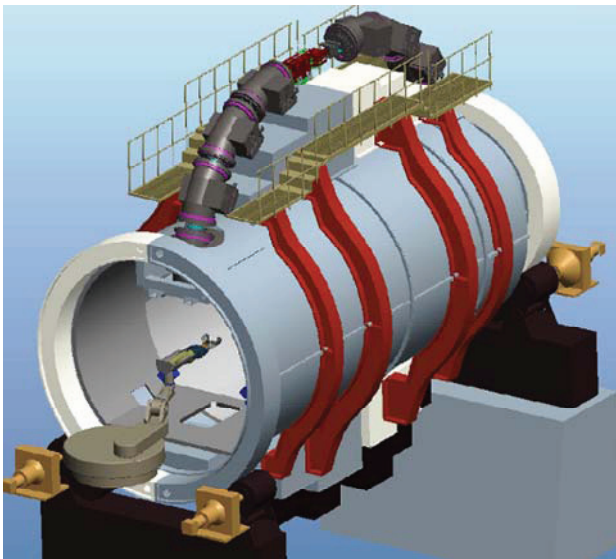
Figure 7: Three-dimensional image of the super-conducting rotating gantry for carbon therapy.

this, it is required to change, the beam energy successively by an energy step corresponding to the water range of 1 or 2 mm. Since the maximum and minimum energies, as used in the raster-scanning irradiation, are 430 and 56 MeV/u, respectively, the synchrotron patterns having the 201 flattops will be needed to cover the entire energy range. Fig. 5 shows a current pattern of the main bending magnets having the 201 flattops.

Beam acceleration and extraction tests using the 201-flattop patterns were successfully made as shown in Fig. 6. In the test, we found that any of the 201 flattops can be extended, and that the beam can be extracted during the

extended flattop. Hence, with this operation pattern having the 201 flattops - *the universal pattern*, the depth dose-distribution could be controlled without using any energy degrader.

SUPERCONDUCTING ROTATING-GANTRY

A three-dimensional image of the isocentric rotating gantry for the new treatment facility is presented in Fig. 7. This rotating gantry has a cylindrical structure with two large rings at both ends. The end rings support the total weight of the entire structure, and are placed on turning rollers so as to rotate the beam line on the rotating gantry along the central axis over ±180 degrees. Carbon beams, provided by the HIMAC, are transported with ten sector-bending magnets, mounted on the gantry structure through each of their supporting structures; they are directed on a target located at the isocenter. In the treatment room, a tumour in a patient is precisely positioned to the isocenter by using a robotic couch.

Layout and beam optics

A layout of the compact rotating-gantry is presented in Fig. 8. The rotating gantry has ten superconducting magnets (BM01-10), a pair of the scanning magnets (SCM-X and SCM-Y), and two pairs of beam profile-monitor and steering magnets (ST01-02 and PRN01-02). A total length and radius of the rotating gantry is 13 m and 5.45 m, respectively. All of these devices are installed and mounted on the cylindrical structure. Since beam focusing can be made only with the combined-function
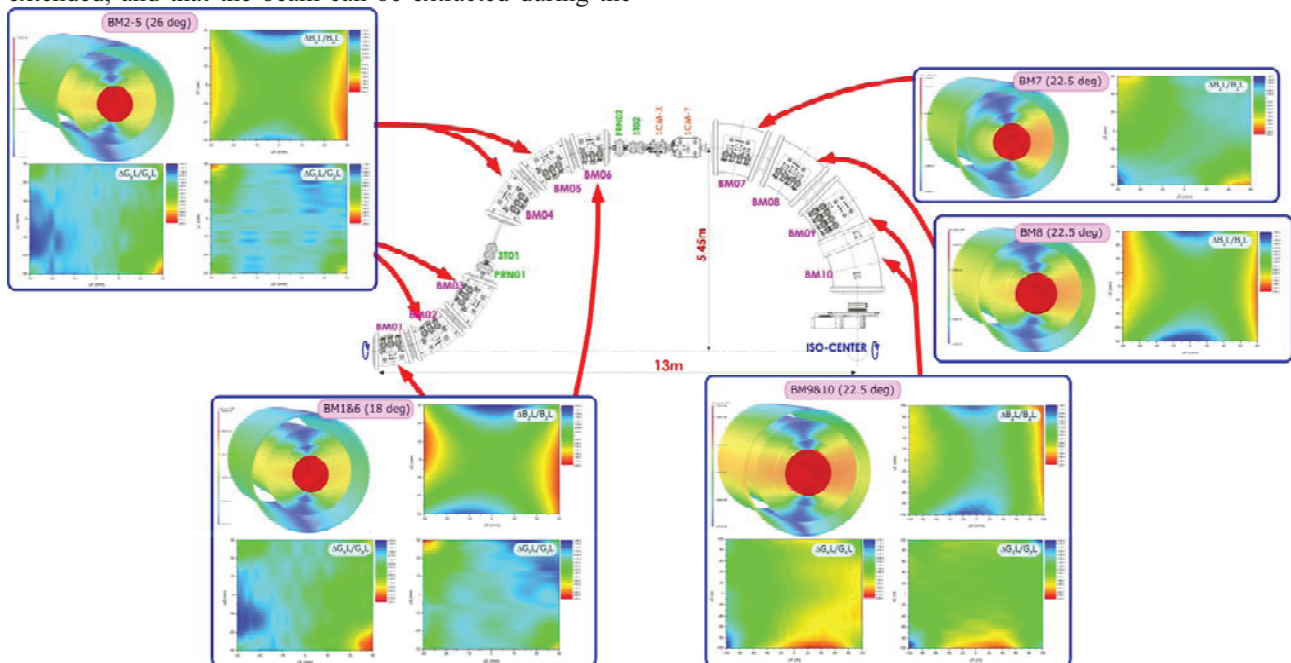

Figure 8: Layout of the superconducting rotating gantry. The gantry consists of ten combined-function superconducting magnets (BM01-10), a pair of the scanning magnets (SCM-X and SCM-Y), and two pairs of beam profile-monitor and steering magnets (ST01-02 and PRN01-02). Representative results of 3D magnetic field calculations for the five kinds of the superconducting magnets are also shown.

Figure 9: Picture of the test bench during rotation tests of the model superconducting-magnet.

superconducting magnets, no quadrupole magnets are needed to install in the rotating gantry, and thus we could design the compact rotating gantry. Details of the beam optics are provided in Ref. [4].

Field calculations

Based on the design of the beam optics, specification of the superconducting magnets was determined. According to their apertures, the magnets are categorized into five kinds. All the magnets have the surface-winding coil structure, and were designed by using a 3D electro-magnetic field-solver, the Opera-3d code [5]. In the code, the curved superconducting coils, having typically a few thousand turns per pole, as well as the cold yoke and vacuum chamber were precisely modelled, and a three-dimensional magnetic field was calculated. Representative results of the calculations are shown in Fig. 8. Having optimized the conductor position, we obtained the required uniformity of the calculated field.
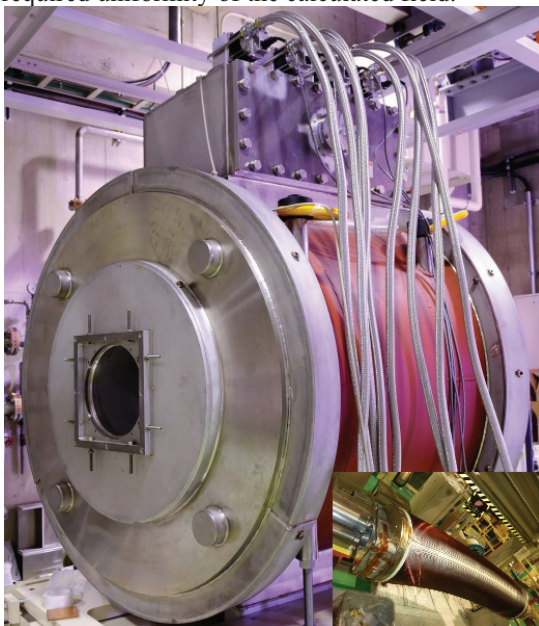

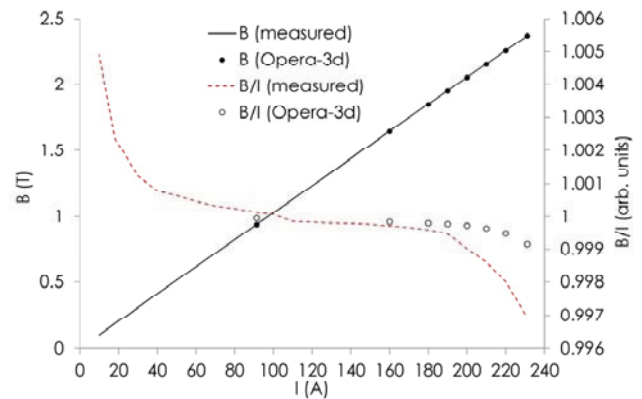Figure 10: Picture of BM10 and its superconducting coil.

Figure 11: Measured magnetic field, *B*, and magnetic field as divided by coil current, *B/I*, as functions of coil current, *I*, for BM10. For comparison, calculated magnetic field is shown by the filled and open dots.

Rotation tests

Since the superconducting magnets on the rotating gantry are to be rotated over ±180 degrees during treatments, an unexpected quench of the superconducting magnets, as caused by rotations, is a concern. To verify this, a model superconducting magnet was developed and tested by Toshiba Corporation. This model magnet has a similar magnet structure as that of BM01-06, although this model magnet only has a dipole coil. Fig. 9 shows a picture of a test bench during rotation tests. Prior to the tests, the coil of the model magnet was cooled down to below 4K by cryocoolers, installed on the magnet. While exciting the superconducting coil with the maximum current, the model magnet was rotated by ±180 degrees, and the coil temperatures in the magnets were monitored. As a result, no unexpected temperature increase, which may cause quench problems, was observed.

Magnetic field measurements

The five superconducting magnets of BM01-BM04 and BM10 (Fig. 10) were constructed, and the rest of the five will be constructed within a year. Firstly, we measured central magnetic field by using an NMR probe. The NMR probe was installed in the middle of the magnet, and current of between *I*=10-240 A was applied for the dipole
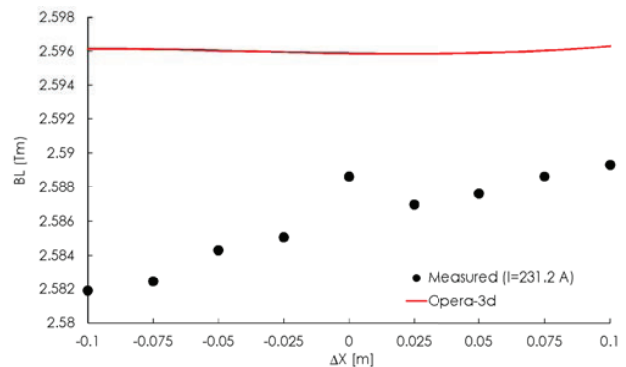

Figure 12: Measured BL products as a function of *ΔX*. Current for the dipole coil is *I*=231.2A. The solid curve show calculated result with the Opera-3d code.
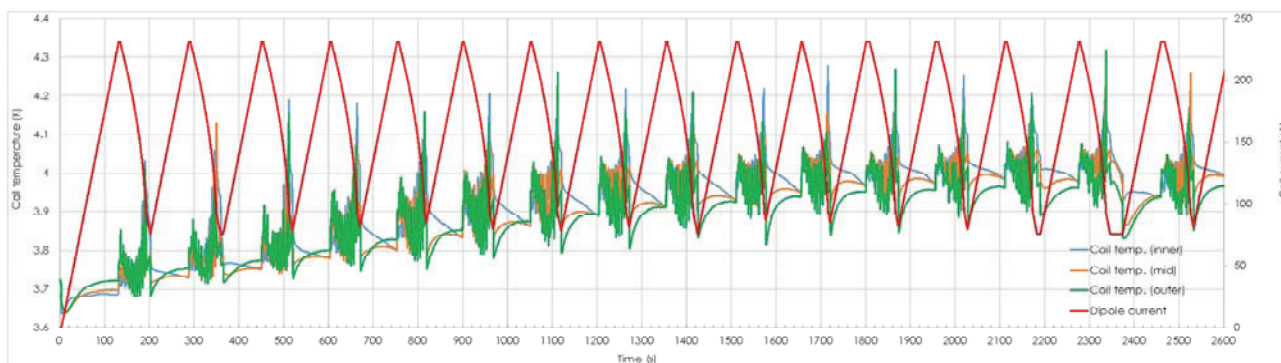
Figure 13: Results of the fast slewing tests for BM10. Average coil temperatures were converged below 4K.

coil of BM10. The measured magnetic field, *B*, and magnetic field as divided by the coil current, *B/I*, are shown by the solid and dashed curves in Fig. 11, respectively. For comparison, calculated results of *B* and *B/I* using the Opera-3d code are also plotted by the filled and open dots in Fig. 11, respectively. We found that the measured and calculated magnetic field agreed with each other, although the measured *B/I* curve at the maximum current slightly differs with the calculated curve. This discrepancy might be attributed to a difference in estimation of a packing factor for the laminated cold yoke.

Secondarily, measurements of magnetic field distributions along beam trajectories were performed. Measured-magnetic field distributions along the central beam trajectory were measured and integrated over the beam trajectories to determine a *BL* product and an effective length. The same analysis was made for the calculated distribution with the Opera-3d code. Fig. 12 shows the *BL* products of various beam trajectories, as shifted horizontally by ΔX, for the dipole current of *I*=231.2A. Here, the values of the *BL* products are normalized, so as to have the same effective length of $L=\rho\theta$=2.8m×22.5° for all the trajectories. Corresponding results, as calculated by the Opera-3d code, are also shown by the solid curves in the figures. The absolute values of the measured *BL* agreed with the calculated values within accuracy of a few times 10^{-3}; however we clearly see the quadrupole component of approximately $GL\sim3.8\times10^{-2}$ T for the measured field in Fig. 12. We presume that this unexpected quadrupole component might be attributed to an alignment error between the superconducting coil and cold yoke. However, since this magnet has the quadrupole coil, this quadrupole component can be corrected by adding or reducing current for the quadrupole coil by approximately ΔI=5 A from the applied quadrupole current of $I\sim200$ A.

Fast slewing tests

To simulate the multiple flattop operation, fast slewing tests were made. In the tests, currents of both the dipole and quadrupole coils were maximized to initialize the magnet, and then were decreased by 201 steps. In each step, coil currents were kept for 0.3 s, where carbon beams would be extracted from accelerators and transported through a beam-transport line including the

rotating-gantry during this constant-current region. Further, the coil temperatures were measured with resistance temperature sensors, installed in the inner, middle and outer sides of the coil. A representative result for BM10 is provided in Fig. 13. Although the coil temperature gradually increases, we found that the average coil temperatures were converged around 4 K, while the critical temperature is approximately 6.8 K.

SUMMARY AND FUTURE PLAN

Recent developments of the HIMAC accelerator complex are reported. To take advantage of the fast raster-scanning irradiation, the multiple energy operation was developed. This operation using 11-flattop pattern was successfully commissioned, and is presently used in scanning-treatment operations. Furthermore, we successfully made beam acceleration and extraction tests with 201-flattop pattern, which enables us to perform the full energy scanning; this operation will be used for treatment operation in near future.

A compact superconducting rotating-gantry for carbon therapy is being developed. Having optimized the layout using the combined-function superconducting magnets, we could design the compact rotating-gantry. The design study as well as major tests of the superconducting magnets was completed, and the construction of the superconducting rotating-gantry is in progress. The rotating-gantry will be completed at the end of FY2014, and be commissioned in FY2015.

ACKNOWLEDGMENT

REFERENCES

[1] K. Noda, *et al.*, Nucl. Instrum. and Meth. in Phys. Res. B 266 (2008) 2182.

[2] T. Furukawa, *et al.*, Med. Phys. 37 (2010) 5672.

[3] Y. Iwata, *et al.*, Nucl. Instrum. and Meth. in Phys. Res. A 624 (2010) 33.

[4] Y. Iwata, *et al.*, Phys, Rev. ST Accel. Beams 15 (2012) 044701.

[5] Opera Version 16, http://www.cobham.com/.